ELSEVIER

Wear 252 (2002) 595–606

WEAR

www.elsevier.com/locate/wear

An investigation of the tribological properties of thin KCl films on iron in ultrahigh vacuum: modeling the extreme-pressure lubricating interface

G. Wu [a], F. Gao [a], M. Kaltchev [a], J. Gutow [b], J.K. Mowlem [a], W.C. Schramm [c], P.V. Kotvis [d], W.T. Tysoe [a,*]

[a] *Department of Chemistry and Laboratory for Surface Studies, University of Wisconsin-Milwaukee, P.O. Box 413, Milwaukee, WI 53211-0413, USA*
[b] *Department of Chemistry, University of Wisconsin-Oshkosh, Oshkosh, WI 54901, USA*
[c] *PVI Systems, 78 Howard Street, New London, CT 06320, USA*
[d] *Benz Oil Inc., 2724 Hampton Avenue, Milwaukee, WI 53209, USA*

Received 16 July 2001; received in revised form 2 January 2002; accepted 10 January 2002

Abstract

The frictional properties of thin KCl films deposited onto clean iron are measured in ultrahigh vacuum using a tungsten carbide tribotip, where the observed initial rapid decrease in friction coefficient with film thickness is proposed to be due to the formation of a complete KCl monolayer where the friction coefficient of this film is ∼0.27. A 1800 Å thick KCl film shows a hardness and friction coefficient similar to those for bulk KCl when the width of the surface height distribution of the tribotip measured by atomic force microscopy (AFM) is 2000–3000 Å. This implies that the KCl film behaves like the bulk material when the film thickness exceeds the roughness of the interfaces.

Keywords: KCl; Iron; Auger spectroscopy; Scanning electron microscopy; Atomic force microscopy; Friction coefficient; Extreme-pressure lubrication; Ultrahigh vacuum tribometer

1. Introduction

We have previously shown that chlorinated hydrocarbons thermally decompose during extreme-pressure lubrication at the hot, lubricated interface to deposit a film that consists of $FeCl_2$ and carbon [1,2] where interfacial temperatures in excess of 1000 K can be attained [3]. It was also shown that the resulting interfacial coefficient of friction depended on the chlorinated hydrocarbon that was used as an additive, with films incorporating larger amounts of carbon apparently having larger interfacial coefficients of friction. Raman spectroscopy revealed that the carbon was present, in these cases, as small (∼50 Å) diameter particles [4].

Carbon tetrachloride was found to be a particularly effective lubricant additive [5]. This efficacy was traced to the formation of a carbide film and it was found that the tendency to form carbides increased with the presence of additional chlorine on the surface [6]. Similar carbides were found when chloroform was used as an additive at higher concentrations and was manifested by an increase in seizure load at higher additive concentrations [7]. Thus, the nature of the lubricating interface that is formed when using chlorinated hydrocarbon additives is relatively complicated and depends on the nature of the additive and the tribological conditions, consisting of a film of $FeCl_2$+carbonaceous particles formed on a substrate that incorporates various amounts of carbon. It was also found that it was possible to reproduce plots of seizure load versus additive concentration by assuming that the wear rate was given by the Archard equation [8–11]. It has also been shown that chlorinated hydrocarbons [12] and sulfur-containing molecules [13] thermally decompose on iron in ultrahigh vacuum to form the same surface films and with identical growth kinetics, as those formed at higher pressures.

In order to explore the friction and wear behavior of inorganic boundary films and to provide a well-characterized interface that can be probed in detail, we have investigated the tribological properties of thin KCl films deposited onto clean iron. This model system is simpler than the $FeCl_2$+C/Fe+C surface that is formed by reaction of a chlorinated hydrocarbon with iron. An understanding of these simpler model systems will help in understanding the tribological properties of more complicated, reactively formed films. These tribological experiments were carried out in ultrahigh vacuum to provide well-defined substrates and films, and to avoid

* Corresponding author. Tel.: +1-414-229-5222; fax: +1-414-299-5036.
E-mail address: wtt@uwm.edu (W.T. Tysoe).

0043-1648/02/$ – see front matter
PII: S0043-1648(02)00009-1

effects due to surface contamination. The advantage to this strategy is that it completely eliminates atmospheric contamination and also allows well-characterized samples to be synthesized. It also allows the nature of the film and the substrate to be varied in a systematic way enabling differences in the properties of the film and substrate to be explored. The initial experiments, described in the following, focus on thin KCl films deposited onto a clean iron substrate. The use of a pure iron substrate will subsequently allow the effect of carbon solution in the iron to be investigated in a systematic way. A simple model for the friction coefficient of a uniform thin film of shear strength (S_f) deposited onto a flat substrate of hardness (H_s) has been proposed by Bowden and Tabor [14] and Merchant [15], and suggests that the friction coefficient should be given by:

$$\mu = \frac{S_f}{H_s} \tag{1}$$

A KCl film was selected since it will not react with the iron substrate and has a relatively low hardness ($H_{Knoop} = 7.2$ [1 1 0] and 9.3 [1 0 0]) and therefore, low shear strength [14], so that, based on the simple Bowden and Tabor theory [14] should provide a relatively low friction coefficient film.

2. Experimental

Experiments were carried out in an 8 in. diameter ultra-high vacuum chamber pumped using a combination of an ion and sublimation pump operating at a base pressure of 5×10^{-10} Torr following bakeout. An iron foil (0.1 mm thick, Johnson–Matthey, 99.99% purity) was polished to a mirror finish using 1 μm diamond paste. The foil was then spot-welded to a 0.25 mm thick steel plate to provide a rigid base for the sample. This was mounted onto a vacuum-compatible sample manipulator allowing the sample to be moved in the *x*, *y* and *z* directions and rotated about its axis. The sample could be resistively heated and the sample temperature was monitored using a thermocouple spot-welded to the back of the steel plate support. The sample manipulator was mounded horizontally on the vacuum chamber and opposite the vacuum tribometer. This allowed the sample to be moved to the center of the chamber for Auger analysis using a cylindrical-mirror analyzer incorporated into the chamber or tribological experiments to be carried out. The sample could also be retracted from this position to allow the tribometer pin to be interrogated using Auger spectroscopy. Finally, the sample could be placed in front of an ion bombardment source for sample cleaning.

The vacuum tribometer (Fig. 1) consisted of a tribopin mounted to the end of an arm that could be moved horizontally (in the *x* and *y* directions) and also vertically (in the *z* direction), either toward or away from the sample, which is oriented horizontally during tribological experiments. These motions were controlled by external servomotors, which allowed the pin position to be precisely determined and normal (*z* direction) and lateral (*x* direction) forces were monitored by strain gauges mounted to thinned sections of the triboarm. The strain gauges were calibrated by hanging weights from the arms. The tribopin was mounted to the end of the arm using a chuck which allows pins of different materials and diameters to be substituted relatively easily. The experiments reported below were carried out using a tungsten carbide pin cut from a ball bearing (diameter 1.27 cm).

The tribometer was under computer control (using LabView software) which allowed the arm to be moved to any desired location and also to be retracted away from the center of the chamber. The software also allowed the conditions for the experiment to be set. These included applied load, scan speed and pattern. Finally, the tribotip was electrically attached to an MHV connector which allowed the resistance between the sample and tribotip to be monitored. This connector was also used to heat the tribopin using electron bombardment by means of a retractable filament that could be moved close to the tribopin while it was being heated or moved away to allow tribological experiments to be performed.

The top port of the vacuum chamber included an ion bombardment source for sample cleaning, a KCl evaporation source and a viewport. The iron foil was cleaned using a literature protocol [16] that consisted of argon ion bombardment (1 μA/cm^2, 3 keV), primarily to remove carbon and sulfur, and then annealing at ~1000 K in vacuo to remove volatile surface contaminants. This resulted in further carbon and sulfur diffusion from the bulk, which was then removed by additional ion bombardment cycles.

The potassium chloride evaporation source was constructed based on a literature design [17] in which KCl (Aldrich, 99.9% purity) was placed in a small alumina tube (diameter 0.5 mm, 1 cm long) and wrapped by a tantalum heating wire. This was supported on copper rods and mounted onto a 2.75 in. conflat flange. In order to obtain reproducible evaporation rates, it was found crucial to monitor the temperature of the KCl. This was done by inserting a chromel/alumel thermocouple into the KCl pellet. This was read via feed-throughs in the 2.75 in. flange and allowed a particular evaporation rate to be selected merely by changing the pellet temperature.

The chamber also incorporated a Hiden HAL 301/3F quadrupole mass spectrometer that was used to monitor the cleanliness of gases introduced into the chamber, for leak testing and for monitoring products that might evolve during tribological testing. A single-pass, cylindrical-mirror analyzer was placed such that it could be used to analyze the iron sample and the tribopin. Auger spectra were typically collected using an incident current of 0.1 μA at an energy of 3 keV using a modulation amplitude of 1 V. The first derivative signal from the lock-in amplifier was plotted versus electron kinetic energy and monitored using a computer. Note that Auger spectroscopy must be used with great care when scrutinizing halides since they are strongly affected by the electron beam [18].

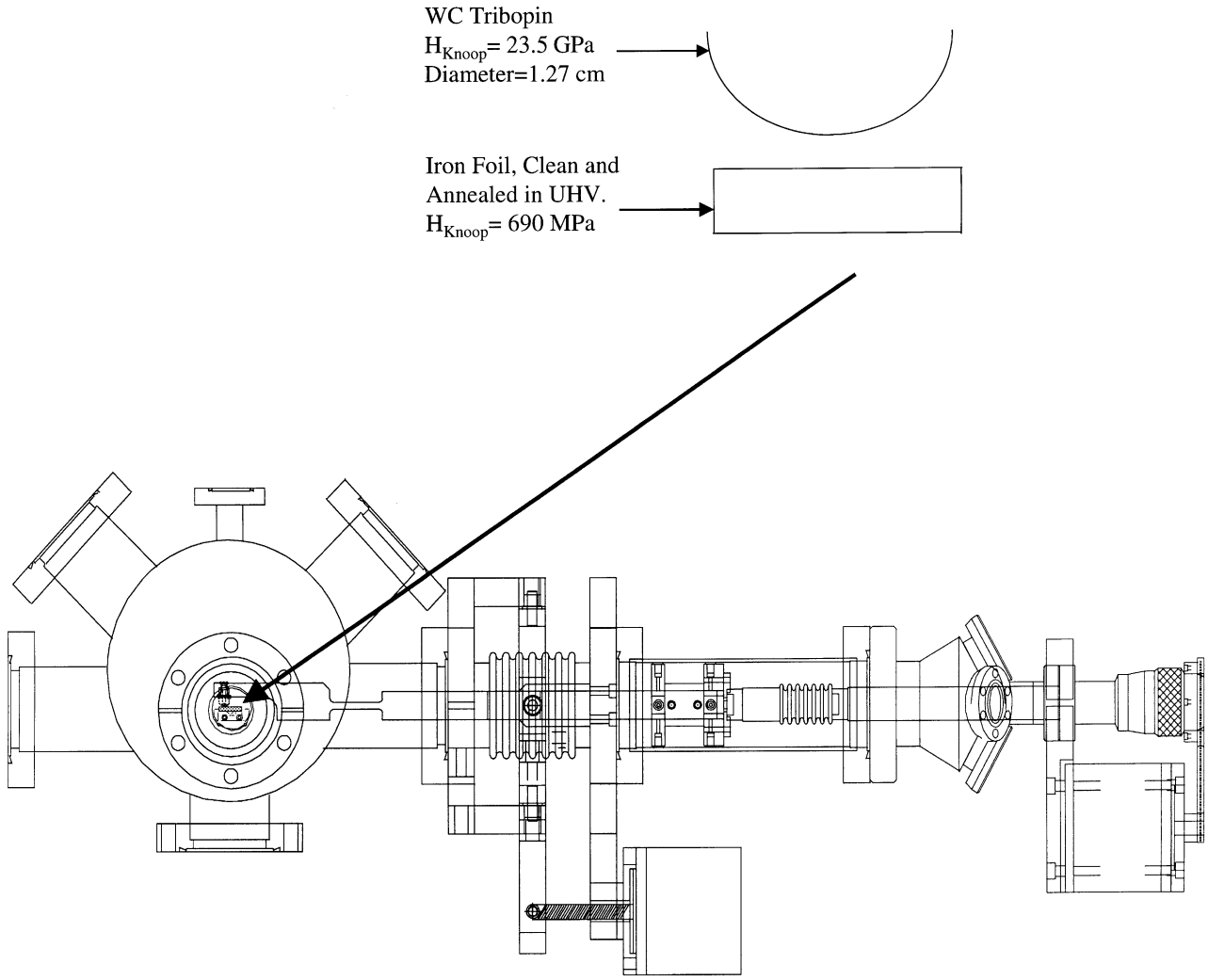

Fig. 1. Diagram of the ultrahigh vacuum tribometer. Shown also is the geometry of the tribopin and iron foil substrate.

The KCl film was monitored using X-ray photoelectron spectroscopy in another chamber that has been described in detail elsewhere [19] or in situ using a quartz crystal thickness monitor (Sigma Instruments, model SQM-160). The halide film is not susceptible to damage by the X-ray beam. X-ray photoelectron spectra were collected using Mg Kα radiation using a power of 130 W. The resulting photoelectrons were analyzed using a double-pass, cylindrical-mirror analyzer operating at a pass energy of 50 or 100 eV. These were detected by a channeltron operating in pulse-counting mode.

Electron micrographs were collected using a Topcon model SM-300 electron microscope equipped with an EDAX detector.

Atomic force microscopy (AFM) images of the tribopin were collected ex situ using a Park Scientific AutoProbe SPM using a 100 μm scanner. Images were collected in contact mode using a gold-coated SiN cantilever (sharpened microlever A) with a radius of curvature of <20 nm and a spring constant of approximately 0.05 N/m. The contact force was set to 2.5 nN. Scans (256×256 pixels) were collected at a rate of two lines per second over an area of 26.4 μm on a side. Images were processed minimally to correct for sample tilt by subtracting a plane from the image. Image processing was performed using the IGOR software package by Wavemetrics rather than the instrument manufacturer's software. Images were collected at a minimum of three different locations on each sample. Due to the tribopin curvature, it was not possible to make measurements at locations more than approximately 50 μm apart. The sharpened part of the tip is only 200 nm tall with a cone angle of 18° (a base width of approximately 130 nm) meaning that the tip may not have penetrated to the bottom of deep crevasses.

Knoop microhardnesses were measured using a Buehler Micromet II microhardness tester. Loads, unless otherwise specified, were 1.96 N using indentation times of 12 s.

3. Results

3.1. Characterization of the pin and iron surfaces

The polished iron foil sample was cleaned using a combination of argon ion bombardment and annealing in vacuo. The cleanliness of the iron sample was monitored using Auger spectroscopy. Small amounts of residual sulfur, carbon and nitrogen were detected after several cleaning cycles but each corresponded to <3% of a monolayer [20]. A scanning electron microscopy (SEM) image of the surface after polishing and cleaning in vacuo is displayed in Fig. 2a. No discernible surface topography is revealed by this image, consistent with the sample treatment. The Knoop hardness of the clean and annealed iron sample (measured after removal into air) was 70 ± 1 (equivalent to $6.9 \pm 0.1 \times 10^8$ Pa).

Displayed in Fig. 2b is a SEM image of the surface of the tungsten carbide ball. Some surface defects are noted in this image and the pin appears rougher than the iron sample (Fig. 2a). An EDAX of the pin is also shown in the figure (Fig. 2c). This technique, because of the high energy electrons used, is not very surface sensitive and reveals that the pin contains tungsten carbide with cobalt used as a binder. The literature value for the hardness of WC is 2.35×10^{10} Pa [21] and is much larger than that of the pure iron ($6.9 \pm 0.1 \times 10^8$ Pa).

3.2. Growth and characterization of the potassium chloride films

Potassium chloride was evaporated onto clean iron in ultrahigh vacuum using the evaporation source described

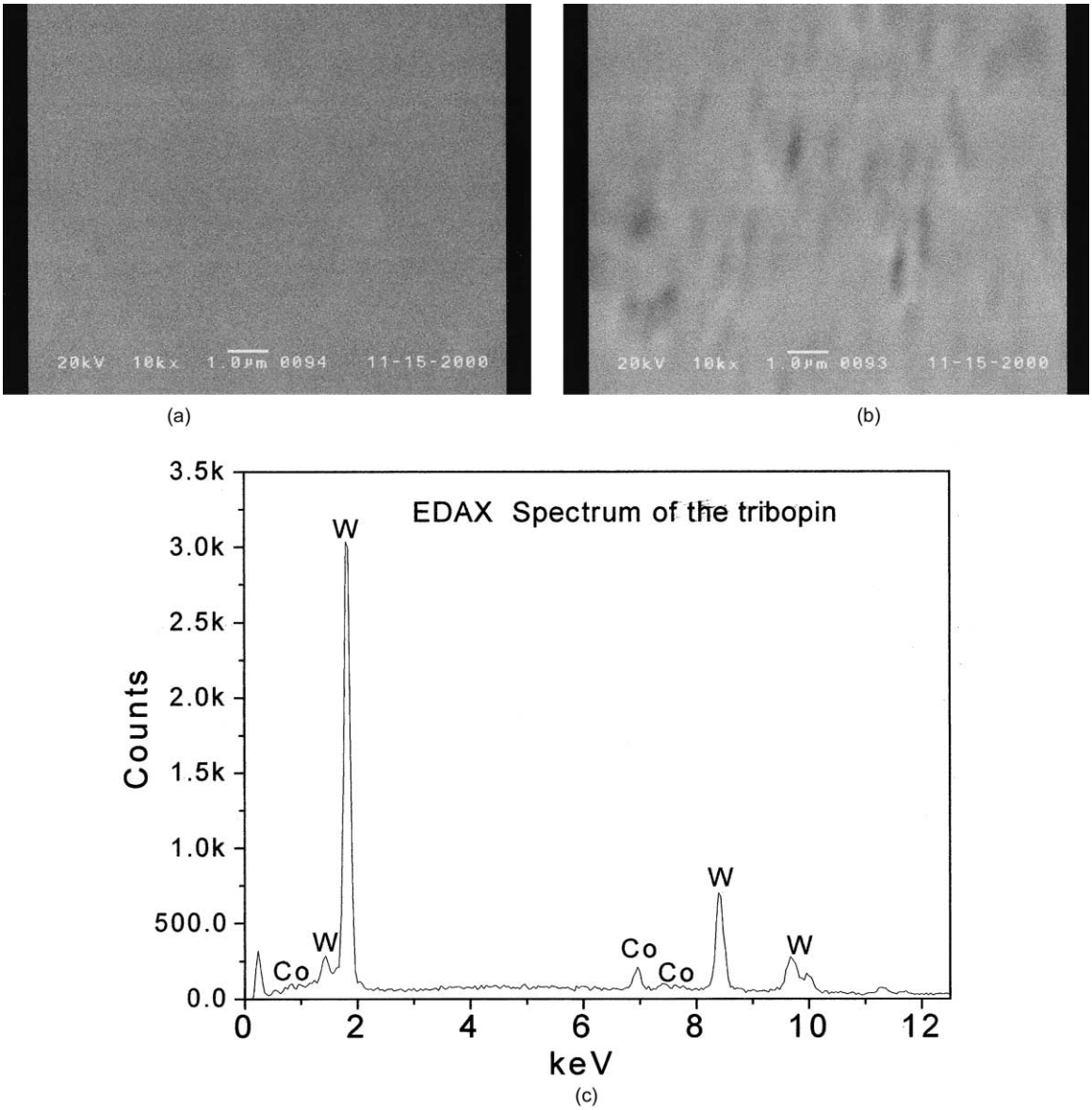

Fig. 2. SEM images of (a) the clean iron foil, (b) the tungsten carbide tribopin and (c) an EDAX spectrum of the tribopin.

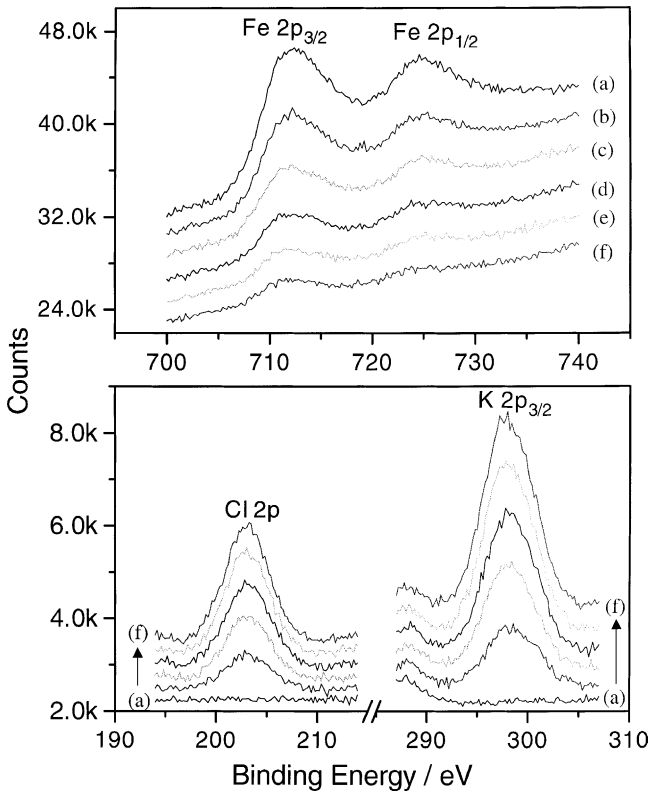

Fig. 3. X-ray photoelectron spectra of the KCl film and the iron substrate as a function of KCl deposition time. Spectra (a) are of the clean surface and (b–f) represent increasing KCl deposition times.

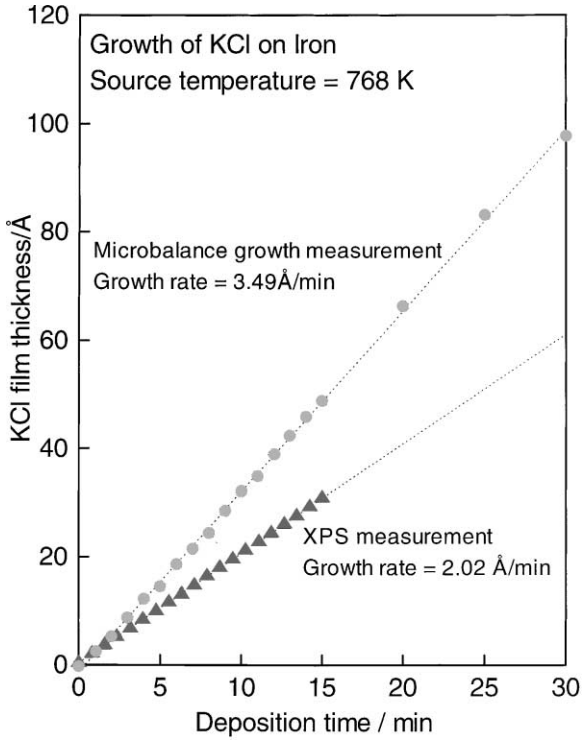

Fig. 4. Plot of film thickness versus time for the evaporation of KCl onto clean iron in ultrahigh vacuum. The film thickness was measured either using the relative intensities of the iron, potassium and chlorine X-ray photoelectron signals and the electron escape depths (▲) or by using the quartz microbalance (●).

above. Shown in Fig. 3 is a series of X-ray photoelectron spectra of films of KCl grown on an iron foil as a function of deposition time. Potassium is indicated by the feature at 298.2 ± 0.2 eV binding energy (K 1s state) and confirms the presence of potassium in a +1 oxidation state [22]. This binding energy remains constant even for very thin KCl layers. Similarly, the presence of chlorine is indicated by the 1s photoemission state at 203.0 ± 0.2 eV binding energy indicating the presence of Cl^-. Again, this feature does not shift with coverage suggesting the presence of KCl on the surface over the whole coverage range. Finally, the relative intensities of these features indicates a 1:1 stoichiometry as expected for the deposition of KCl [23]. The iron substrate is indicated by the presence of features at 712.3 ± 0.2 and 725 ± 0.2 eV binding energies and the absence of any other features due, for example, to oxygen or carbon indicates that pure films are deposited onto the surface.

The film thickness was estimated from the variation in intensity of the chlorine or potassium features compared to those of iron using standard electron escape depths [23]. This model leads to an exponential decrease in the iron signal and a corresponding exponential increase in the signals due to chlorine and potassium. Typical results for this analysis, using a pellet temperature of 768 K, are displayed in Fig. 4 which show the film thickness plotted versus time (▲). The film thickness was also measured using a quartz crystal microbalance (●) included in the tribometer chamber. These results are also plotted onto the data of Fig. 4 which reveal that X-ray photoelectron spectroscopy underestimates the amount of material deposited onto the surface and indicates that the films do not grow layer by layer. Subsequent data are plotted using the film thicknesses measured using the quartz crystal microbalance.

3.3. Frictional behavior of KCl films

Shown in Fig. 5 is a typical friction coefficient trace as a function of position along the sample for a scan 4 mm long at a scan speed of 4 mm/s with a load of 0.29 N for a 1800 Å thick KCl film on clean iron. The average value, in this case, is ~0.3 and shows variations above and below this value. These are not due to noise in the collections system and are inherent in the frictional measurement and may be due to some stick–slip behavior. Friction coefficients quoted below represent an average over the whole scan and error bars represent the extent of deviation from this measurement. Note that the friction coefficient remains constant throughout the scan. This behavior is found for all film thicknesses.

A plot of the friction coefficient versus KCl film thickness measured using a load of 0.29 N for sliding speeds of 8 mm/s is displayed in Fig. 6a. Data were also collected at a sliding speed of 4 mm/s and identical friction coefficients

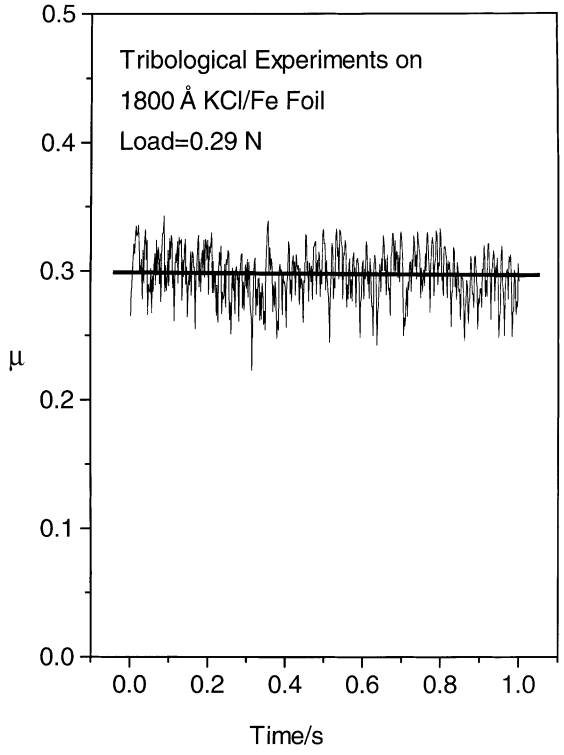

Fig. 5. A typical friction coefficient trace as a function of position along the sample for a scan 4 mm long using a tribopin that had been heated to ∼1000 K at a scan speed of 4 mm/s using an applied load of 0.29 N for a 1800 Å thick KCl film deposited onto iron.

were obtained. These data were collected for several different samples using a tribopin that had not been heated in vacuo. These results show that the friction coefficient of the WC pin on the clean iron surface is 2.4 ± 0.3. The addition of a KCl film of 10 Å in thickness causes a substantial decrease in the friction coefficient to 1.6 ± 0.1 and the addition of more KCl causes a further decrease, so that the minimum friction coefficient (0.25 ± 0.05) is attained at a film thickness of ∼90 Å. As more KCl is added, the friction coefficient appears to increase slightly with film thickness so that, after the deposition of ∼1700 Å of KCl, the friction coefficient increases to 0.40 ± 0.05. Shown also on this figure is a histogram of the surface topography measured using AFM (Fig. 6b). This shows a relatively narrow height distribution between 0 and 1000 Å from the surface where the width at half height of the distribution is ∼350 Å. Shown also is an Auger spectrum of the unannealed tribopin (Fig. 6c) which reveals that the pin has undergone some air oxidation and also has a large amount of carbon on the surface.

A similar set of data is shown in Fig. 7a but, in this case, for a tribopin that had been heated to ∼1000 K in ultrahigh vacuum between each experiment. This procedure effectively removes any contamination that might have accumulated on the tribopin. No KCl was detected at the tip of the tribopin after measuring the friction coefficient in a single scan. Note, however, that the tip of the pin points downwards while the electron beam passes horizontally, making it difficult to ensure that the end of the pin had been interrogated. However, all subsequent tribological data are collected for a tribopin that had been heated in vacuo. This plot shows a similar rapid decrease in friction coefficient to a minimum value of 0.23 ± 0.02 after the deposition of 40–90 Å of KCl, in good agreement with the data of Fig. 6a. In this case, however, the friction coefficient remains reasonably constant with increasing film thickness. Displayed in Fig. 7b is the surface topology of the tribopin that had been annealed in ultrahigh vacuum at ∼1000 K and the corresponding Auger spectrum is shown in Fig. 7c. This reveals that the majority of the surface oxide had been removed by heating in vacuo and the spectrum also exhibits features due to the cobalt binder. The roughness of the surface appears to have increased substantially due to heating in vacuo. Neither the change in surface topology nor the change in surface composition appears to have had a major effect on the minimum film thickness required to reach the lowest friction coefficient (between 40 and 90 Å).

In order to establish whether the friction coefficient obeyed Amontons' law [24], the friction coefficient was measured as a function of applied load for loads between 0.29 and 1.18 N for a KCl film of thickness 1350 Å at a sliding speed of 4 mm/s and the results are displayed in Fig. 8. These indicate that, within the errors of each measurement, the friction coefficient remains essentially constant with increasing applied load so that it obeys Amontons' law over the range of loads tested.

Phase-contrast optical micrographs were collected of the wear scars on clean iron after a single scan, as a function of applied load, using a sliding speed of 4 mm/s with an annealed tribopin. Typical results of the apparent contact area (calculated as $\pi W^2/4$, where W is the wear scar width) are shown in Fig. 9. These data were collected for several iron samples and the results were in good agreement with the data shown here. The slope of this plot is 280 ± 20 MPa.

Similar measurements can be made for surfaces covered with films of KCl. A typical plot of contact area (measured using phase-contrast micrographs of the wear scar) versus applied load, in this case for an iron sample covered by 1350 Å of KCl, is shown in Fig. 10a. This plot is linear within experimental error. Also displayed in Fig. 10b is an atomic force micrograph of a wear scar of an iron foil covered by 1350 Å of KCl formed with an applied load of 0.29 N. The widths of the scars measured from the AFM image and phase-contrast optical microscopy are in excellent agreement. This shows that the KCl film away from the scar is relatively smooth as expected from the topology of the iron film. It appears that material is deposited around the wear track at a relatively large distance away in small fragments.

The slopes of graphs such as that shown in Fig. 10 are plotted versus KCl film thickness in Fig. 11. Shown for comparison are the Knoop hardnesses of pure iron and KCl. Finally, the friction coefficient of a pure KCl disk was measured at an applied load of 0.29 N in high vacuum using the same tribometer and yielded a value of 0.30 ± 0.05.

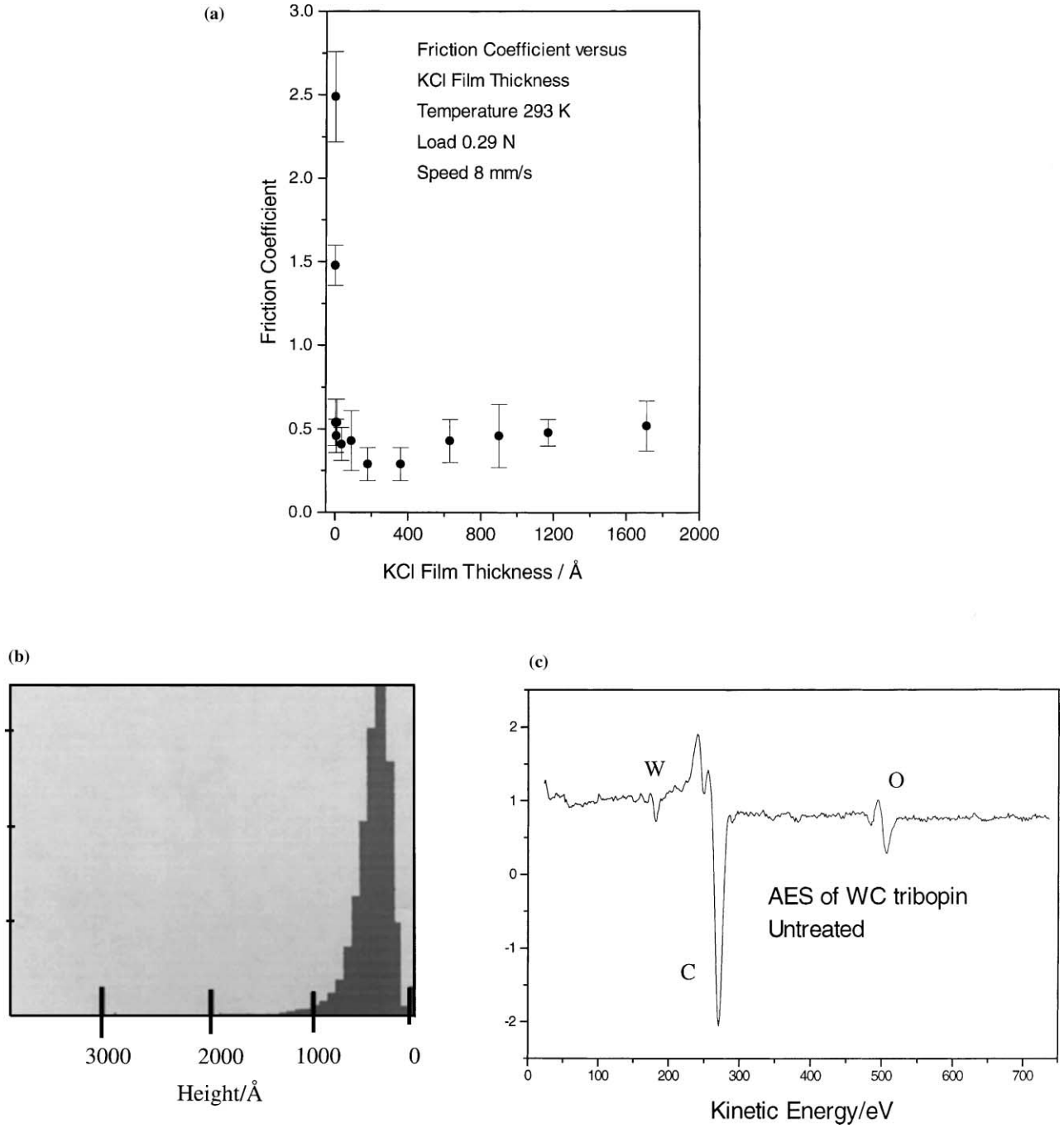

Fig. 6. (a) Plot of friction coefficient versus KCl film thickness following deposition onto clean iron in ultrahigh vacuum with a sliding speed of 8 mm/s (●) using a load of 0.29 N at 293 K using the tribopin as-received following a clean solution, (b) a histogram of the topology of the tribopin and (c) an Auger spectrum of the tribopin.

The contact resistance between the tribopin and the sample was also monitored while collecting the friction coefficient data [10]. The results, plotted as $\log_{10}$ (contact resistance) versus film thickness, are shown in Fig. 12 using a sliding speed of 4 mm/s and an applied load of 0.29 N, with an annealed tribopin and thus correspond to the friction coefficient data shown in Fig. 7. For film thicknesses up to ~50 Å, the contact resistance is very close to the value of the clean surface. Note that the resistance of the external circuit has not been subtracted from these data and this likely contributes to a large fraction of this resistance. The contact resistance increases drastically for larger thicknesses and values for KCl films thicker than ~800 Å are above the detectability limit of the apparatus (since the digital to analog convertor used to collect the data saturates at a value of ~32 kΩ).

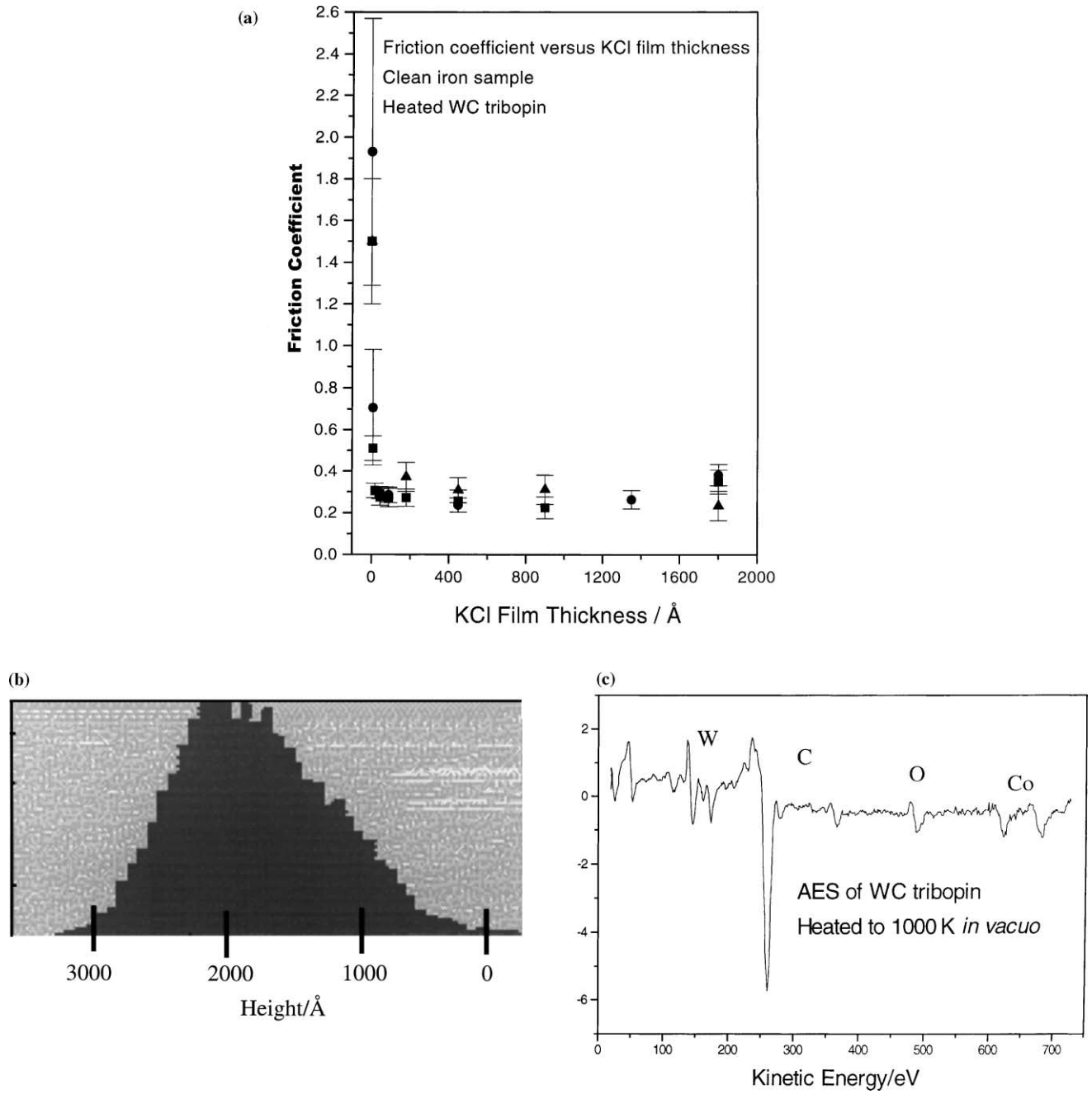

Fig. 7. (a) Plot of friction coefficient versus KCl film thickness following deposition onto clean iron in ultrahigh vacuum with a sliding speed of 4 mm/s using a load of 0.29 N at 293 K using a tribopin that had been annealed in ultrahigh vacuum at ~1000 K, (b) a histogram of the topology of the tribopin and (c) an Auger spectrum of the tribopin.

4. Discussion

4.1. Limiting frictional properties of thick films

The data of Fig. 7 indicate that the friction coefficient drops rapidly with the deposition of ~50 Å of KCl and then remains constant at larger film thicknesses. Comparison with the data of Fig. 6 indicates that this behavior is not sensitive to changes in pin morphology. As the film grows, it will eventually become sufficiently thick that it behaves like the bulk material and be insensitive to the nature of the substrate. In order to explore this transition from a thin- to thick-film regime, the slopes of plots of $\pi W^2/4$ versus load (shown in Figs. 9 and 10a) are plotted versus film thickness (Fig. 11). The slope increases from ~280 MPa for the clean iron surface to ~350 MPa with a 400 Å KCl film present and then monotonically decreases with increasing film thickness to a value of ~120 MPa for a film ~1800 Å thick. A similar

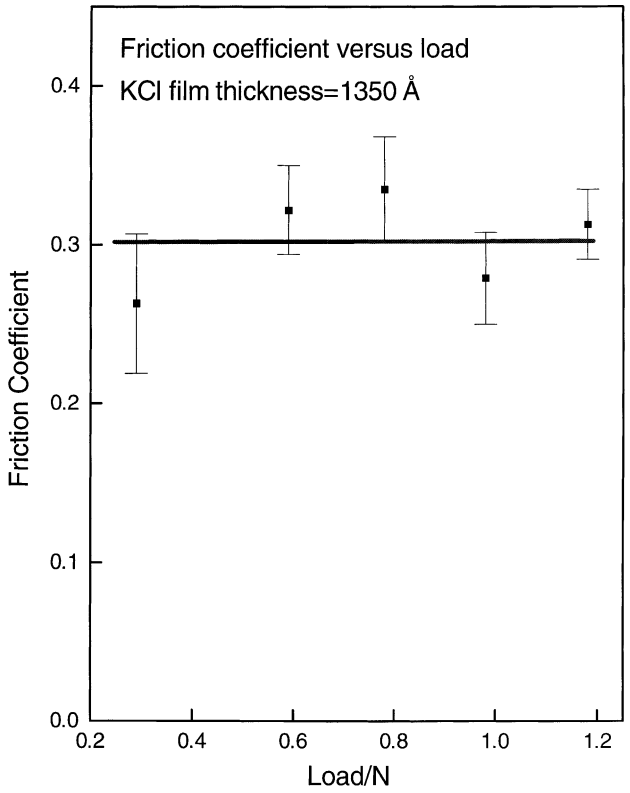

Fig. 8. Plot of friction coefficient versus applied load for a KCl film of 1350 Å in thickness on clean iron using a sliding speed of 4 mm/s.

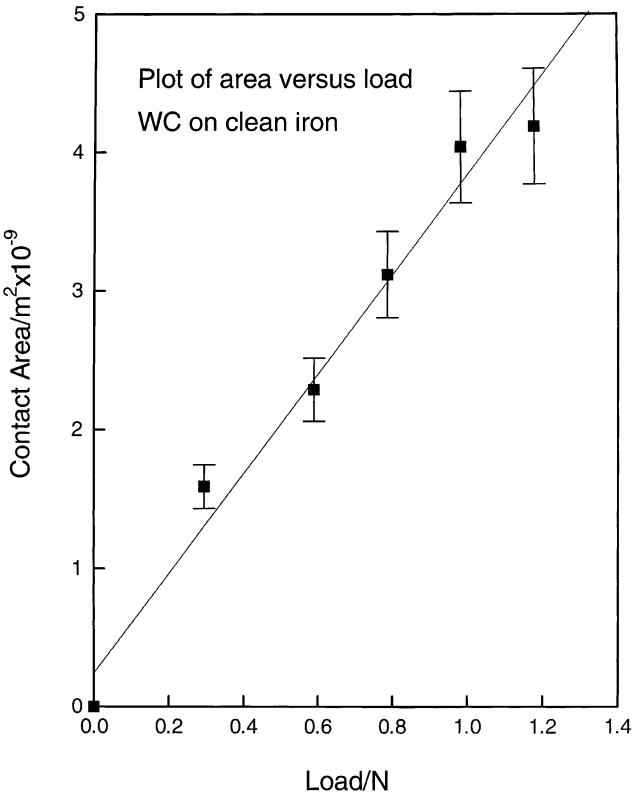

Fig. 9. Plot of contact area versus load for the annealed tribopin sliding on clean iron at 293 K using a sliding speed of 4 mm/s.

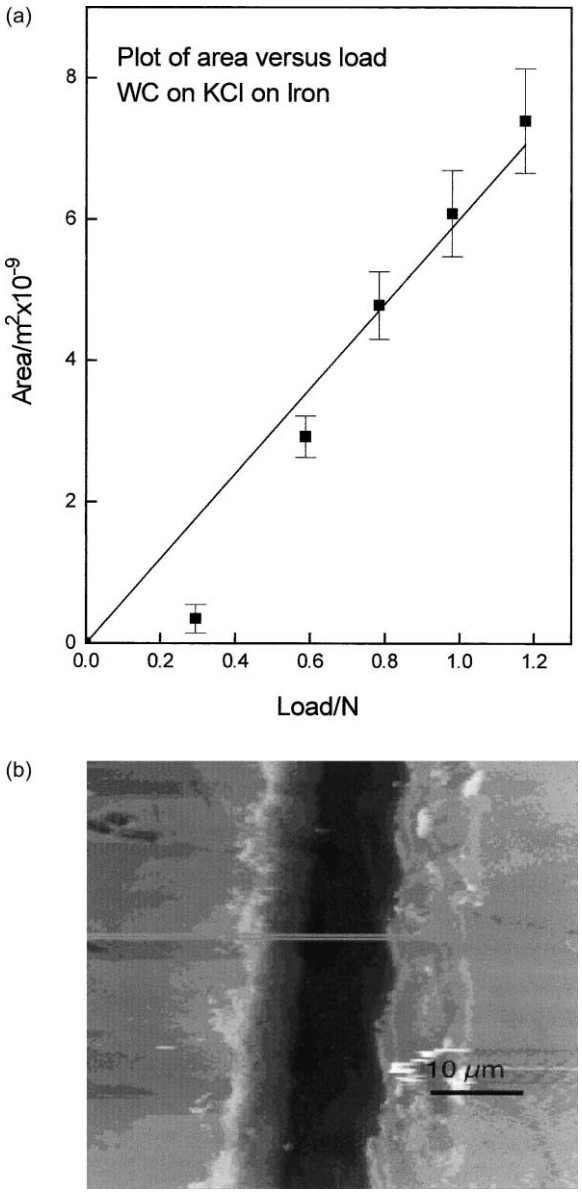

Fig. 10. (a) Plot of contact area versus load for the annealed tribopin sliding on iron covered by 1350 Å of KCl, taken at a sample temperature of 293 K using a sliding speed of 4 mm/s and (b) AFM image of the wear scar for KCl film 1350 Å thick, at an applied load of 0.29 N at a sliding speed of 4 mm/s.

measurement for bulk KCl yields a slope of ~80 MPa so it appears that the values for films of ≥2000 Å and larger are approaching the value for the bulk material. This implies that the mechanical properties of a KCl film of ~2000 Å in thickness are approaching those of the bulk material. It is interesting to note that this value also agrees well with the Knoop hardness of KCl and suggests that all of the asperities of the tribopin have been completely filled by KCl. The view that the 2000 Å thick film behaves like bulk KCl is corroborated by the observation that the friction coefficient of pure KCl (0.30 ± 0.05) is identical, within experimental

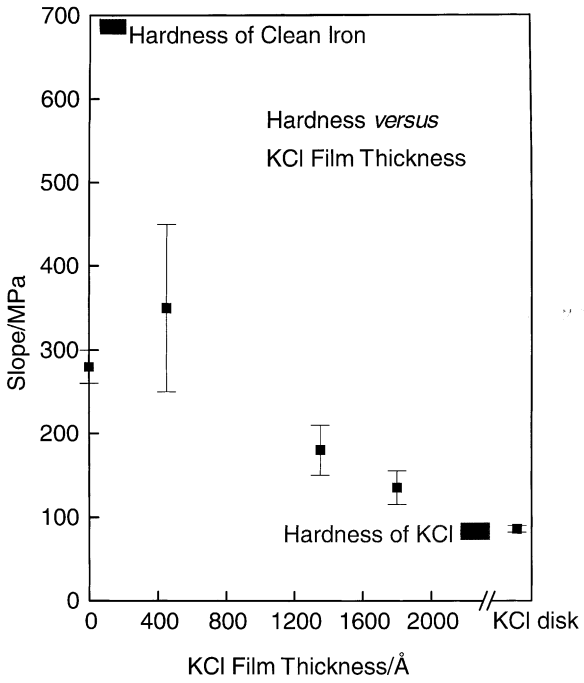

Fig. 11. Slopes of plots of area versus load displayed versus KCl film thickness and on a KCl disk. Indicated for comparison are the Knoop hardnesses (MPa) for the clean and annealed iron foil and for KCl.

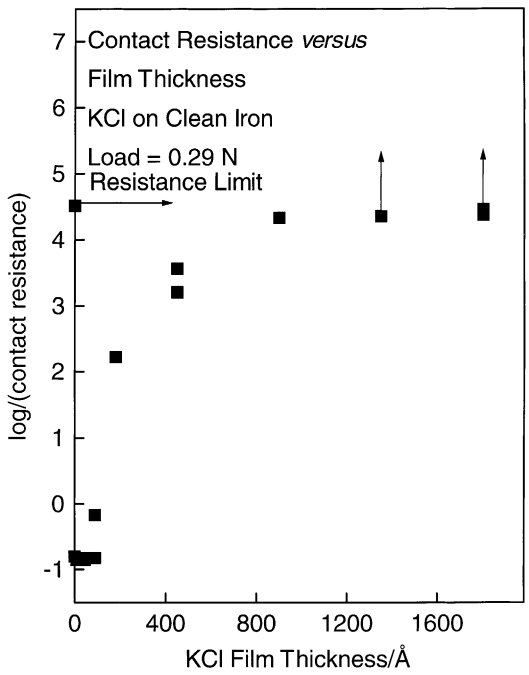

Fig. 12. Plot of $\log_{10}$ (contact resistance) between the tribopin and the surface as a function of KCl film thickness using an applied load of 0.29 N at a sliding speed of 4 mm/s. The maximum resistance that can be measured is indicated by a horizontal line (as "resistance limit").

accuracy, to that of the thick film (0.3 ± 0.1). This notion is in accord with the contact resistance measurements displayed in Fig. 12. This shows that 1400 and 1700 Å thick KCl films have contact resistances >32 kΩ, the upper detection limit of our measurement technique. This thickness of KCl film is of the same order of magnitude at the roughness of the tribopin (Fig. 7b) suggesting that the film behaves like the bulk material when the film thickness exceeds the roughness of the interfaces.

4.2. Tribological behavior of a thin KCl film

The data presented in Figs. 6 and 7 show that the presence of a thin film of 40–90 Å of KCl causes the friction coefficient to decrease to ~0.25, apparently independently of the roughness of the surfaces. This limit, therefore, appears to be controlled by the nature of the KCl film rather than the topology of the contacting surfaces, at least, within the limit of the relatively smooth surfaces investigated in this work. The friction coefficient continues to increase somewhat with increasing film thickness in the case of the data shown in Fig. 6a, while it remains constant with increasing film thickness in the data of Fig. 7a. Since the data of Fig. 7a were collected after cleaning the tribopin by heating to ~1000 K between each experiment, this suggests that the increase in μ for the thicker films in Fig. 6a might be due to the accumulation of contaminants on the tribotip. It should be noted that the different symbols for the data shown in Fig. 7a represent different iron samples in different experiments indicating that the frictional data are extremely reproducible.

It is interesting to note that the friction coefficient remains relatively constant for thicknesses between 90 and 1800 Å (Fig. 7a). It is clear, however, that the film does not display bulk-like properties for films <400 Å thick (Fig. 11). KCl is likely to be relatively immobile on an surface at 300 K, so that the formation of second, third and subsequent KCl layers is likely to proceed during deposition, before the first layer has saturated. This view is corroborated by the data of Fig. 4 which show that film thicknesses measured using X-ray photoelectron spectroscopy are substantially lower than those measured directly using the microbalance, in accord with the view that the KCl is not growing layer by layer. It is proposed that the initial minimum in the friction coefficient data presented in Fig. 7a, at a film thickness of ~50 Å is coincident with the saturation of the first monolayer by KCl. Note that this does not imply that this first layer is ~50 Å thick but that second, third and subsequent layers are formed before the first layer is completed so that the total film thickness at this point is ~50 Å. In order to test the notion that covering the iron by a single layer of KCl reduces the friction to its minimum value, we assume the resultant friction coefficient to be proportional to the relative coverages of clean iron and KCl. Writing the coverage of KCl as Θ, where $0 < \Theta < 1$, then:

$$\mu = \mu^0_{\mathrm{KCl}}\Theta + \mu^0_{\mathrm{Fe}}(1 - \Theta) \quad (2)$$

where μ^0_{KCl} is the friction coefficient of the KCl monolayer and μ^0_{Fe} is the friction coefficient of clean iron. Assuming that the rate of KCl adsorption onto the bare metal in the first layer is proportional to the area of the exposed metal surface yields a rate of adsorption proportional to $1-\Theta$ and is via Langmuir kinetics [25], where integration gives:

$$\Theta = 1 - e^{-\alpha t} \tag{3}$$

where α is a constant. Substituting Eq. (3) into Eq. (2) yields:

$$\mu - \mu^0_{KCl} = (\mu^0_{Fe} - \mu^0_{KCl})\, e^{-\alpha t} \tag{4}$$

Since, according to the data of Fig. 4, the incident flux is constant, the film thickness is proportional to the time, Eq. (4) also represents the theoretical change in friction coefficient as a function of film thickness. The data of Fig. 7a are re-plotted in Fig. 13 as $\mu - \mu_0$ versus film thickness t (■), where μ_0 is taken to be 0.27 ± 0.03. In cases where more than one measurement of the friction coefficient was made for the same KCl film thickness in different runs, these values have been averaged and the resulting error bars included on the figure. These values decrease rapidly and a fit to the function in Eq. (4) is shown plotted as a solid line onto these data using a value of $\alpha = 0.39 \pm 0.02$ Å^{-1}, where the agreement between the experimental data and theory is good. This result is consistent with the idea that the reduction in friction coefficient is caused by the first monolayer of KCl to a limiting value of ~0.27 when this layer reaches saturation. Note that this analysis implicitly assumes that no substantial transfer of material occurs at the interface for these thin films. Since the friction coefficient remains constant through the scan (Fig. 5), this implies that the effect is minimal. Also, as noted above, no KCl was detected on the tip of the tribopin following a single pass. This experiment is, however, not conclusive since we may merely have failed to interrogate the tip of the pin in the small region where the film might exist. Also plotted in Fig. 13 is the predicted coverage of the first monolayer as a function of KCl film thickness (- - -). As noted above, film growth continues in second and third layers prior to the completion of the first monolayer. This shows that the first monolayer is almost complete after the deposition of 40 Å of KCl (where only 0.01% of the surface is bare metal) and Θ becomes exactly unity when 70 Å of KCl has been evaporated. This observation is in accord with the contact resistance measurements of Fig. 12. Here the contact resistance remains low for films less than ~50 Å thick, due to pin–substrate contact because of the presence of an incomplete first layer. At higher KCl film thicknesses, the contact resistance rises steeply implying that the monolayer has been completed in accord with the plot in Fig. 13 derived from the frictional data. The increase between 50 and 800 Å may be due to some breakthrough of the film. These results are, therefore, in accord with the notion that the first monolayer substantially reduces the interfacial friction coefficient and is remarkably robust. A similar friction reduction has also been found for chemisorbed overlayers deposited onto clean single crystal samples in ultrahigh vacuum [26,27].

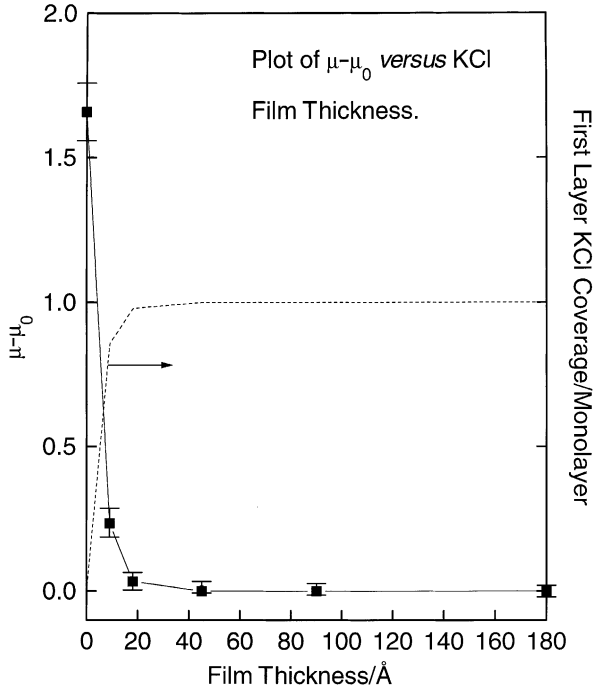

Fig. 13. Plot of $\mu - \mu_0$ versus KCl film thickness following deposition onto clean iron in ultrahigh vacuum with a sliding speed of 4 mm/s using a load of 0.29 N at 293 K using a tribopin that had been annealed in ultrahigh vacuum at ~1000 K (■). Shown as a solid line is a fit to these data. Shown also is the KCl coverage in the first monolayer calculated using the model (- - -).

As shown in Eq. (1), the lateral force is assumed to be that required to shear the contacting interface and is given by the shear strength of the interfacial material. This implies that the coefficient of friction for a thin film of KCl (μ) is given by:

$$\mu = \mu_0 \frac{S_{KCl}}{S_{Fe}} \tag{5}$$

where μ_0 is the friction coefficient for clean iron (1.9 ± 0.3) and S_{KCl} and S_{Fe} the respective shear strengths. Shear strengths are difficult to measure but have been calculated using thermodynamic data from the equation [11].:

$$S = 0.427 \left(\frac{L\rho}{3}\right) \ln\left(\frac{T_m}{T}\right) \tag{6}$$

where ρ is the density (g/cm^3), L the latent heat of fusion (cal/g), T_m and T the melting point and temperature (K) and S the shear strength (kg/mm^2) [28]. Substituting the resulting values into Eq. (6) yields a value of $\mu = 0.24 \pm 0.04$. An alternative approach is to realize that the shear strength is proportional to the hardness [14]. This has been measured for the iron and is $6.9 \pm 0.1 \times 10^8$ Pa. The Knoop hardness of KCl is 7.2 kg/mm^2 (7.06×10^7 Pa) along [1 1 0] or 9.3 kg/mm^2 (9.12×10^7 Pa) along [1 0 0]. The former value predicts $\mu = 0.19 \pm 0.03$ and the latter value $\mu = 0.25 \pm 0.04$. All of these calculated values are in good agreement with each

other and, more important, in agreement with the limiting value of 0.27 ± 0.03. However, it should be noted that this agreement may be fortuitous since it is difficult to imagine that a monolayer of KCl has the same shear properties as the bulk material. This, however, will be tested by using films of different materials deposited onto the iron surface to see if similar agreement is found in these cases. Note that this model is also consistent with the observation that the friction coefficient is independent of applied load (Fig. 8).

5. Conclusions

Two frictional regimes have been identified. In the first, it is proposed that the initial decrease in friction coefficient is due to the formation of a monolayer of KCl on the surface. Differences in film thicknesses measured using X-ray photoelectron spectroscopy and a quartz microbalance suggest that KCl adsorption, at an iron sample temperature of 300 K, is relatively immobile so that second and subsequent layers are populated before that first layer has saturated. The initial decrease in friction coefficient is mimicked by assuming that the first monolayer of KCl is responsible for the initial decrease in friction coefficient and that adsorption into this layer is via Langmuir kinetics. This suggests that the first layer does not completely saturate until approximately 50 Å of KCl has been deposited. This is in accord with contact resistances measured between the tribopin and the iron surface which remain low for film thicknesses below ∼50 Å and increases rapidly for thicker films. Measurement of the wear scar width versus applied load suggests that the film properties mimic those of bulk KCl when the film thickness becomes of the order of or greater than the surface roughness. This view is corroborated by the observation that ∼1800 Å thick KCl film has the same friction coefficient as bulk KCl and the contact resistance at this point is infinite.

Acknowledgements

We gratefully acknowledge support of this work by the Chemistry Division of the National Science Foundation, under grant number CHE-9213988. We also thank M. Maclaurin for help with collecting SEM and EDAX data.

References

[1] T.J. Blunt, P.V. Kotvis, W.T. Tysoe, Tribol. Trans. 41 (1998) 117.
[2] T.J. Blunt, P.V. Kotvis, W.T. Tysoe, Tribol. Trans. 41 (1998) 129.
[3] T.J. Blunt, P.V. Kotvis, W.T. Tysoe, Tribol. Lett. 2 (1996) 221.
[4] L. Huezo, P.V. Kotvis, C. Crumer, C. Soto, W.T. Tysoe, Appl. Surf. Sci. 78 (1994) 113.
[5] J. Lara, H. Molero, A. Ramirez-Cuesta, W.T. Tysoe, Langmuir 12 (1996) 88.
[6] P.V. Kotvis, J. Lara, K. Surerus, W.T. Tysoe, Wear 201 (1996) 10.
[7] W.T. Tysoe, K. Surerus, J. Lara, T.J. Blunt, P.V. Kotvis, Tribol. Lett. 1 (1995) 39.
[8] J.F. Archard, J. Appl. Phys. 24 (1953) 981.
[9] E. Rabinowitz, Friction and Wear of Materials, Wiley, New York, 1965.
[10] R. Holm, Electric Contacts, Almquist & Wiksell, Stockholm, 1946.
[11] H. Ernst, M.E. Merchant, in: Proceedings of the Special Summer Conference on Friction and Surface Finish, M.I.T., 1940, p. 76.
[12] J. Lara, W.T. Tysoe, Langmuir 14 (1998) 307.
[13] M. Kaltchev, P.V. Kotvis, J. Lara, T.J. Blunt, W.T. Tysoe, Tribol. Lett. 10 (2001) 45.
[14] F.P. Bowden, D. Tabor, The Friction and Lubrication of Solids, Oxford University Press, London, 1964.
[15] M.E. Merchant, J. Appl. Phys. 11 (1940) 230.
[16] V.S. Smentkowski, C.C. Cheng, J.T. Yates Jr., Langmuir 6 (1990) 147.
[17] W.J. Wytenburg, R.M. Lambert, J. Vacuum Sci. Technol. 10 (1992) 3579.
[18] M.L. Knotek, P.J. Feibelman, Surf. Sci. 90 (1978) 78.
[19] J. Lara, W.T. Tysoe, Langmuir 14 (1998) 307.
[20] L.E. Davis, Handbook of Auger Electron Spectroscopy, 2nd Edition, Physical Electronics, Eden Prairie, MN, 1979.
[21] ASM Handbook, Vol. 18, American Society of Metals, Cleveland, 1992.
[22] C.D. Wagner, W.M. Riggs, L.E. Davis, J.F. Moulder, G.E. Muilenberg, Handbook of X-Ray Photoelectron Spectroscopy, Perkin Elmer, Eden Prairie, 1979.
[23] S. Hofmann, in: D. Briggs, M.P. Seah (Eds.), Practical Surface Analysis, Wiley, New York, 1983.
[24] G. Amontons, Memoires de l'Academie Royale, A, Chez Gerard Kuyper, Amsterdam, Vol. 1706, pp. 257–282 (1699).
[25] A.C. Clarke, Theory of Adsorption and Catalysis, Academic Press, New York, 1970.
[26] D.H. Buckley, Surface Effects in Friction, Adhesion, Lubrication and Wear, Elsevier, Amsterdam, 1981.
[27] A.J. Gellman, Tribol. Lett. 10 (2001) 39.
[28] R.C. Weast, S.M. Selby (Eds.), Handbook and Chemistry and Physics, Chemical Rubber Co., Cleveland, OH, 1967.